ACS Catalysis

pubs.acs.org/acscatalysis Research Article

Hydrogen Dissociation Controls 1-Hexyne Selective Hydrogenation on Dilute Pd-in-Au Catalysts

Hio Tong Ngan, George Yan, Jessi E. S. van der Hoeven, Robert J. Madix, Cynthia M. Friend,* and Philippe Sautet*

Cite This: *ACS Catal.* 2022, 12, 13321−13333 Read Online

ACCESS | Metrics & More | Article Recommendations | Supporting Information

ABSTRACT: Increasing the selectivity of the catalytic hydrogenation of alkynes to alkenes is of major importance for the processing of petrochemicals and the production of fine chemicals. Achieving high selectivity for alkene formation at high conversions, however, remains a long-standing challenge in heterogeneous catalysis. Here, the mechanism and origin of the high selectivity of dilute Pd-in-Au catalysts has been studied by a combination of first-principles calculations, microkinetic simulations, and isotopic exchange hydrogenation experiments using $Pd_{0.04}Au_{0.96}$ nanoparticles embedded in raspberry colloid-templated silica. The Pd is predominantly in the form of isolated atoms, only surrounded by Au atoms, based on prior studies. The simulations indicate that the rate-limiting process for 1-hexyne hydrogenation on Pd monomers in Au(111) is H_2 dissociation, which has a large free energy barrier of 0.86 eV at 363 K and 0.2 bar of H_2. The C−H bond formation steps, on the other hand, proceed with lower barriers, which contrasts with previous studies of extended Pd catalysts. The microkinetic simulations identify the sizable H_2 dissociation barrier and the small barrier for the hydrogenation of 1-hexyne as key factors that lead to a high selectivity for the production of 1-hexene from 1-hexyne, even at high conversion. The unconventional H_2 dissociation limiting process in combination with the low coverage of weakly bound hydrocarbon intermediates explains the near-zero order of 1-hexyne found experimentally. Furthermore, the partial hydrogenation of 1-hexyne to form 1-hexene is shown to be an irreversible process from our isotopic exchange hydrogenation experiments and is explained by the strongly exothermic nature of the reaction. Diluting active species, like Pd, in a less active host metal, like Au, hence appears promising as a means of tuning the binding energy of reactants and altering reaction profiles, leading to distinct kinetic behavior for an optimal catalytic activity and selectivity. The combination of microkinetic modeling, density functional theory calculations, and isotopic exchange experiments is thus demonstrated to be an effective approach to modeling important catalytic phenomena.

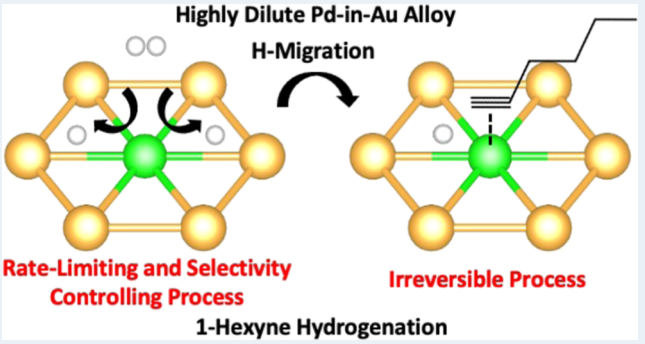

KEYWORDS: *catalysis, dilute alloy, selective hydrogenation, 1-hexyne, palladium, gold, density functional theory, microkinetic simulations*

INTRODUCTION

Selective hydrogenation is an essential process in the fine chemicals and petrochemical industries. Selective hydrogenation of specific functional groups, such as −C≡C, −C=O, $-NO_2$, and −COOH(R), is often required for the production of fine chemicals.[1] Likewise, selective hydrogenation is critical in the removal of alkynes, which poison catalysts for downstream polymerization in the petrochemical industry.[2]

The partial hydrogenation of alkynes to selectively form alkenes with high conversion is a long-standing challenge in heterogeneous catalysis. Ideally, 100% conversion with 100% selectivity for alkene formation would be achieved. The Lindlar catalyst, which has a high concentration of Pd and is supported on $CaCO_3$ (5 w/w % $Pd/CaCO_3$), is now widely used for alkyne hydrogenation;[3] however, the selectivity for alkene formation is insufficient. The selectivity of the hydrogenation of 2-hexyne to 2-hexene on this catalyst, for example, is only ∼88% at ∼25% conversion.[4] Alkynes have stronger binding to the Pd catalyst surface than alkenes;[5−7] hence, most of the active sites of the catalyst are occupied by the alkyne molecules when the conversion is low.[8] The strong adsorption of alkynes eliminates the alkene molecules from the catalyst surface and prevents overhydrogenation, which enhances the selectivity.[9] However, when the conversion is high, the selectivity deteriorates. Quinoline and lead are added to the Lindlar catalyst to improve both activity and selectivity.[4] Because lead

Received: July 21, 2022
Revised: October 5, 2022
Published: October 18, 2022

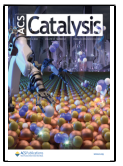

https://doi.org/10.1021/acscatal.2c03560
ACS Catal. 2022, 12, 13321−13333

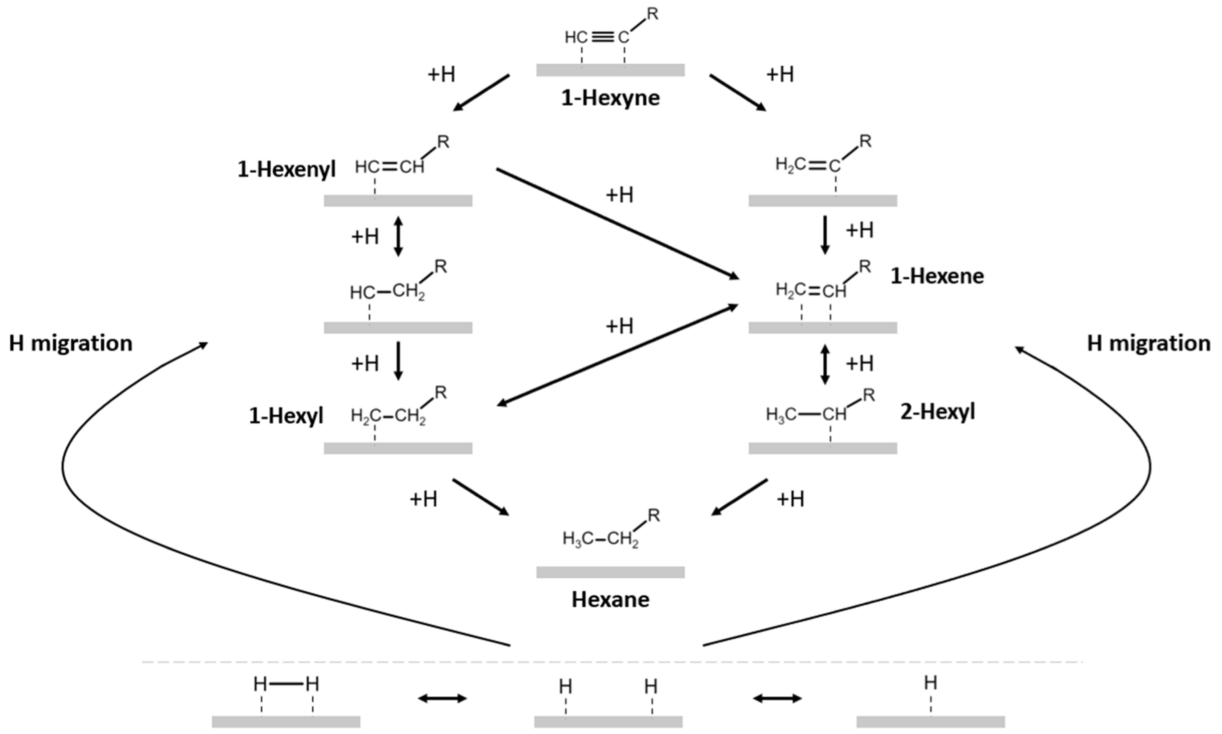

Figure 1. Schematic representation of the course of 1-hexyne hydrogenation. The bottommost pathway shows H_2 dissociation and subsequent migration to supply H atoms for 1-hexyne hydrogenation on another $Pd_1Au(111)$ site. 1-Hexyne can be hydrogenated either by fully hydrogenating one of the two unsaturated carbon atoms followed by the remaining one (left) or by alternately hydrogenating the two carbon atoms (right). The former is detrimental to selectivity as it skips 1-hexene formation and produces hexyls directly through 1-hexylidene. Double-headed and single-headed arrows indicate reversibility and irreversibility, respectively, based on experiments and theory in this paper.

is extremely toxic, there is a drive to develop a more selective and environmentally friendly catalyst.

An alternative approach to increase selectivity is to employ dilute alloy catalysts in which an active element, such as Pd, is diluted in a less active metal, such as Cu, Ag, and Au.[10−13] The concept is that the active metal will initiate the catalytic cycle—H_2 dissociation in the case of hydrogenation—whereas the majority, less reactive metal imparts the selectivity by electronically modifying the dilute dopant, compared to its bulk state. In the single-atom limit, the reactive dopant element Pd in the surface layer of Au(111) or Ag(111) has a narrow d-band due to the poor orbital mixing between the two different species.[14,15] This unique electronic structure decreases the covalent binding strength of molecules on the catalyst surface,[16,17] which could be utilized to facilitate alkene desorption over further reaction for selective alkyne hydrogenation. Side reactions, such as oligomerization, require a larger ensemble of active metals and can also be prevented when using dilute alloy catalysts.[18] Thus, by careful tuning, dilute alloys can enhance catalytic performance if these various factors can be understood and related to changes in activity and selectivity.

Previously, dilute alloys of Pd in Cu, Ag, or Au were used to improve the selectivity for partial hydrogenation of alkynes.[13,19−22] The work herein is motivated by investigations of dilute Pd-in-Au RCT-SiO_2 catalysts, for which high selectivity for 1-hexene formation was retained even at high conversions. In contrast, the selectivity substantially degraded at high conversion for pure Pd. Luneau et al. proposed that the high selectivity for the dilute Pd-in-Au alloys is a consequence of the relatively weak binding of half-hydrogenated 1-hexene (hexyl) to Pd single atoms on the dilute alloy, compared to that of the half hydrogenated 1-hexyne (1-hexenyl), resulting in the preferred β-C−H bond breaking to reform one of the hexene isomers.[8] The rate-limiting step of the 1-hexyne hydrogenation was proposed to be the second hydrogenation step of 1-hexyne.

Herein, the origin of the high selectivity at high conversion of 1-hexyne hydrogenation (Figure 1) catalyzed by a dilute Pd-in-Au catalyst was explored. Theoretical modeling using density functional theory (DFT) and microkinetic modeling were combined with results from isotopic exchange experiments to establish that the rate for alkyne hydrogenation on Pd single atoms embedded in Au is mainly controlled by H_2 dissociation, whereas C−H bond formation is widely thought to be the sole rate-determining step on pure Pd.[23] The sizable H_2 dissociation barrier and small barrier for the hydrogenation of 1-hexyne compared to that of 1-hexene control the selectivity in 1-hexene, enabling a high selectivity even at high conversion. Experiments and theory show that hydrogenation of 1-hexyne is irreversible. The DFT calculations further indicate that hydrocarbon adsorption (1-hexyne and 1-hexene) is considerably weaker on the dilute Pd-in-Au alloy compared to Pd(111) and that the undesired pathway to form 1-hexylidene is not favored, in agreement with previous work.[8,24] These results illustrate a powerful methodology to rationally design new catalysts for selective alkyne hydrogenation using the synergy of advanced theory and carefully designed experiments.

RESULTS AND DISCUSSION

Dissociation of H_2. Dissociation of molecular hydrogen, a required step for alkyne hydrogenation, takes place on both single Pd atoms and small Pd ensembles on the surface, as

https://doi.org/10.1021/acscatal.2c03560
ACS Catal. 2022, 12, 13321−13333

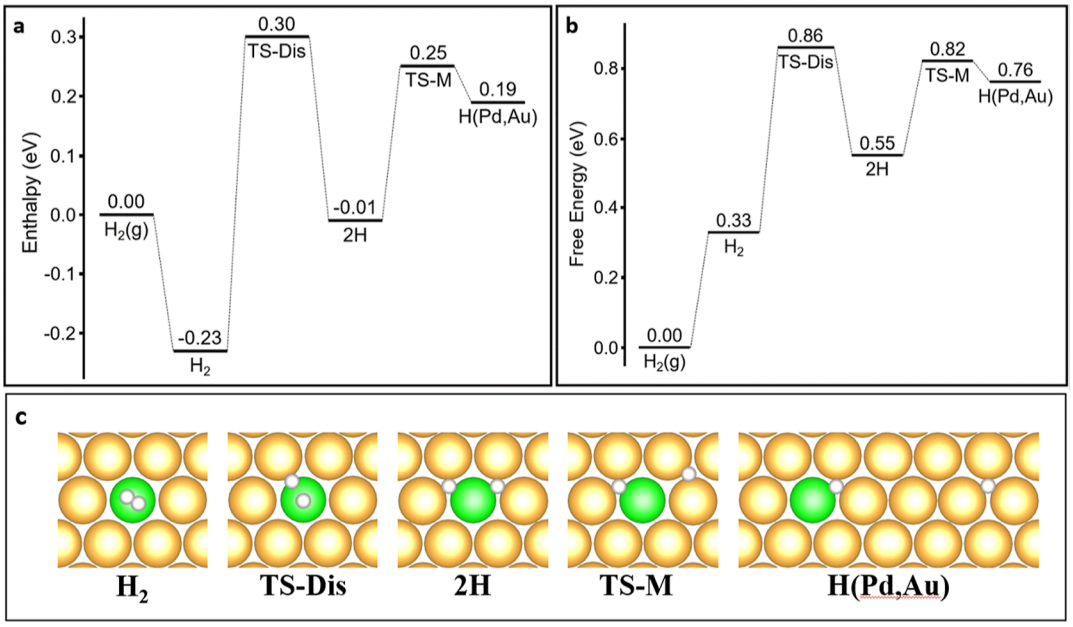

Figure 2. (a) Enthalpy and (b) free energy profiles for hydrogen dissociation and migration on the Pd_1-in-Au(111) surface. All species are chemisorbed, unless indicated by (g) for gas phase species. (c) Structure of each intermediate and transition state along the energy profiles. Conditions used for the free energy calculations are T = 363 K and $P(H_2)$ = 0.2 bar. H_2: molecular adsorption mode of H_2; TS-Dis: H_2 dissociation transition state; 2H: dissociated H_2 into two H atoms adsorbed in Pd_1−Au_2 fcc hollow sites; TS-M: transition state for migration of one H atom toward the Au region; H(Pd,Au): adsorption of one H atom in the Pd_1−Au_2 fcc hollow site and one in the Au fcc hollow site.

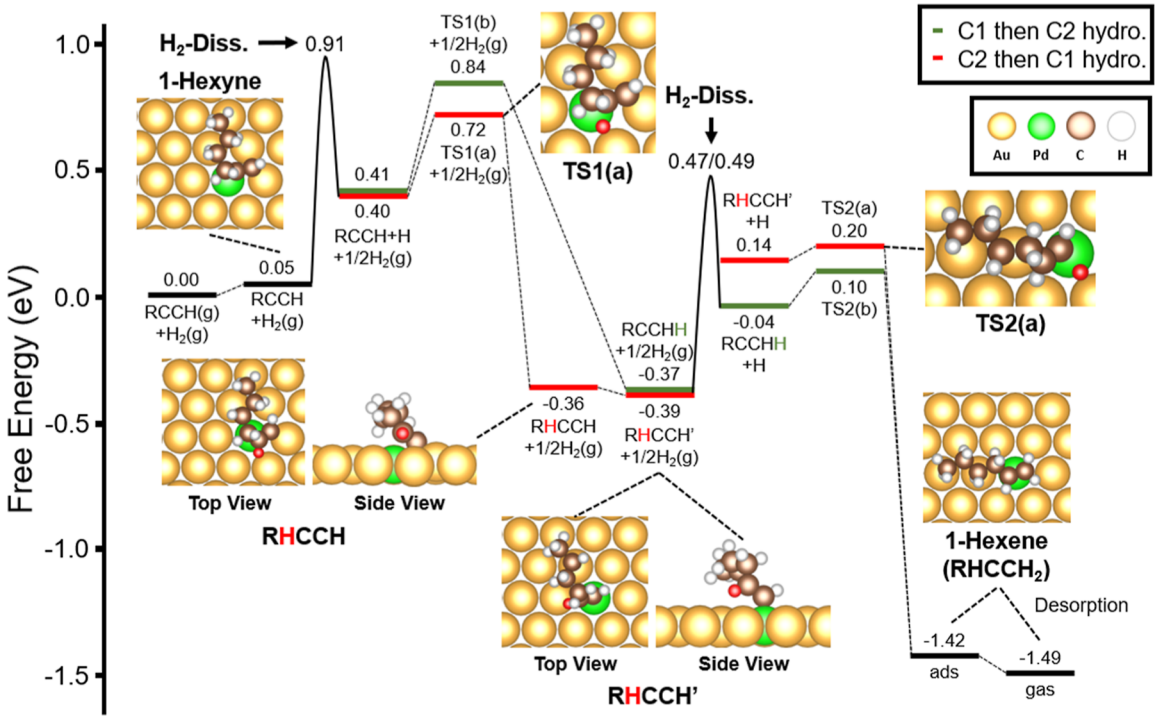

Figure 3. Free energy diagram for 1-hexyne hydrogenation to form 1-hexene on the $Pd_1Au(111)$ surface. The butyl group attached to C≡C bond is abbreviated as R. All species are chemisorbed, unless indicated by (g) for gas phase species. H_2 dissociation occurs on another Pd site, with migration of one H over the Au toward the Pd site where the 1-hexyne is adsorbed. This process (see Figure 2) is lumped into one effective activation barrier of 0.86 eV labeled **H_2-Diss**. The green and red pathways represent the hydrogenation of the terminal carbon atom (C_1) and the carbon atom attached to the butyl group (C_2), respectively, in the first reaction step, followed by the hydrogenation of the remaining carbon atom. The newly added H atoms are indicated in red or green. Reaction conditions are T = 363 K, $P(H_2)$ = 0.2 bar, $P(C_6H_{10})$ = 0.01 bar, $P(C_6H_{12})$ = $P(C_6H_{14})$ = 0.001 bar.

described previously.[25] The calculations included here focus exclusively on Pd monomers embedded in the surface layer of Au(111), hereafter referred to as $Pd_1Au(111)$, because they predominate on the Pd_4Au_{96} catalyst investigated experimentally.[21] The reaction starts with H_2 molecular adsorption [H_2], followed by the transition state of dissociation [TS-Dis] to

https://doi.org/10.1021/acscatal.2c03560
ACS Catal. 2022, 12, 13321−13333

form two separated H atoms [2H] (Figure 2). The enthalpy barrier for H_2 dissociation on the isolated Pd atom is 0.30 eV. The Gibbs free energy (G) barrier is 0.86 eV under the reaction conditions T = 363 K and $P(H_2)$ = 0.2 bar (Figure 2). The resulting structure, with two hydrides bound to the Pd monomer, is metastable with respect to the gaseous H_2 molecules under these conditions. One of the H atoms in the hollow site neighboring the Pd atom can migrate to the Au surface by going through the transition state for migration [TS-M], resulting in the adsorption of one H atom next to the Pd monomer, and one on a pure Au region [H(Pd,Au)]. This detachment of one H atom from the Pd center and migration across the Au surface is activated, but the Gibbs free energy of the transition state (TS-M, G = 0.82 eV) is lower than that of the H−H dissociation step (Figure 2); hence, the dissociation step is overall rate limiting for dissociation of H_2 and migration of H on the alloy surface.[25]

In the following 1-hexyne hydrogenation pathways, the H_2 dissociation and H migration steps will be bundled into a single process with an effective enthalpy barrier of 0.30 eV (and an effective Gibbs free energy barrier of 0.86 eV). The H_2 dissociation energy profile on Pd_1 in Au(111), with a large dissociation barrier and metastable H−H dissociated state, is markedly different from that on the extended Pd(111) surface, on which there is no enthalpy barrier for H_2 dissociation and the dissociated H atoms are stable versus gas phase H_2 in similar conditions.[13] We will show that the sizable barrier for H_2 dissociation on $Pd_1Au(111)$ contributes to the improved selectivity of the alloy catalyst for alkyne hydrogenation. Considering the metastable nature of H on the surface, it is assumed in the presentation of the reaction pathways that one of the two H atoms after dissociation will diffuse and react with 1-hexyne adsorbed at another $Pd_1Au(111)$ site, while the second one will recombine with another surface H atom and desorb as molecular H_2. Hence, one H_2 molecule dissociation event is needed every time an H atom is required to form a C−H bond in the model underlying the free energy profiles. This constraint is lifted for the following microkinetic simulations as all elementary surface reactions are allowed to happen in parallel.

Hydrogenation of 1-Hexyne to 1-Hexene. Hydrogenation of 1-hexyne to form 1-hexene on $Pd_1Au(111)$ is irreversible and is limited by H_2 dissociation (Figure 3). The first step, adsorption of 1-hexyne on the $Pd_1Au(111)$ site, is favorable with an adsorption enthalpy of −1.16 eV, yielding a slightly positive Gibbs free energy of adsorption of +0.05 eV, due to the loss of gas phase entropy. As a result, $Pd_1Au(111)$ active sites are partially covered by 1-hexyne, leaving some sites vacant for H_2 activation. Hydrogenation of adsorbed 1-hexyne can occur when a hydrogen atom is supplied to the adsorbed molecule after H_2 dissociation on another $Pd_1Au(111)$ site followed by H migration. The Gibbs free energy barrier for H_2 dissociation and migration is 0.86 eV as described above (Figure 2), resulting in the co-adsorption of the single H atom and the 1-hexyne molecule (RCCH + H) on a single $Pd_1Au(111)$ site. Notably, the dissociation of H_2 forming two separated H atoms on a $Pd_1Au(111)$ site where a 1-hexyne molecule already resides is less energetically favored than on a bare $Pd_1Au(111)$ site (ΔG_{ads} = 0.77 eV for the former and ΔG_{ads} = 0.55 eV for the latter), meaning that H_2 dissociation hardly takes place on $Pd_1Au(111)$ sites occupied with one 1-hexyne molecule. Dissociation of H_2 and adsorption of 1-hexyne on two different Pd sites with a spillover of one hydrogen though the Au surface toward the 1-hexyne are favored.

There are two pathways for the initial hydrogenation of 1-hexyne: addition of hydrogen to the terminal carbon (C_1, green pathway) and to the second carbon atom (C_2, red pathway in Figure 3) of the C≡C bond. The Gibbs free energy barriers for these first steps are low—0.43 and 0.32 eV for H addition to the C_1 and C_2 positions, respectively. The differences in the barriers are attributed to the greater degree of electron donation from the long carbon chain to C_2; hence, the transition state for C_2 hydrogenation [TS1(a)] has free energy that is 0.12 eV lower than that of the transition state for C_1 hydrogenation [TS1(b)].

The stability of the resulting partially hydrogenated surface species is similar for hydrogenation at either the C_1 or C_2 position (Figure 3). There are two different adsorption structures of the intermediates formed from C_2 hydrogenation: RHCCH is in an η^2 binding mode where carbon C_1 is in a Pd−Au bridge site and C_2 is atop Pd, whereas RHCCH′ is in an η^1 binding mode where only the C_1 carbon interacts atop the $Pd_1Au(111)$ site (see structures in Figure 3). The species formed from C_1 hydrogenation, RCCHH, is in an η^1 binding mode, with C_2 interacting atop the $Pd_1Au(111)$ site (Figure S1). An η^2 adsorption structure resulting from C_1 hydrogenation is not stable, which is attributed to steric hindrance.

Hydrogenation of the partially hydrogenated intermediates, RHCCH′ or RCCHH, is favored over the reverse reaction to reform 1-hexyne on $Pd_1Au(111)$ (Figure 3). Dehydrogenation has a Gibbs free energy barrier of 1.08−1.21 eV, which is higher than the 0.86 eV barrier for the dissociation of a second H_2 molecule. Once an H atom is co-adsorbed with the partially hydrogenated intermediates (RHCCH′+H and RCCHH + H), C−H bond formation proceeds with very low activation barriers, 0.06 and 0.14 eV, respectively. Therefore, the H_2 dissociation and migration step is again rate-limiting. Notably, 1-hexene irreversibly forms, based on the high reverse barrier of at least 1.52 eV. The adsorption of 1-hexene is moderate (ΔH = −1.22 eV, ΔG = +0.07 eV), so that in reaction conditions, desorption of 1-hexene is slightly exergonic (ΔG_{des} = −0.07 eV) and 1-hexene coverage on the catalyst should be low. It should be noted, however, that the adsorption energies of 1-hexyne and 1-hexene are very similar, so that hydrogenation selectivity is not controlled by adsorption competition between these two species, as is the case on bulk Pd catalysts. Our further kinetic simulations are, hence, essential to explain the observed selectivity.

From the DFT free energy profile, the hydrogenation of 1-hexyne to 1-hexene on $Pd_1Au(111)$ is, therefore, predicted to be irreversible and limited by H_2 dissociation with easy C−H bond formation steps. This behavior of single Pd atoms in Au(111) markedly contrasts with the case of pure Pd catalysts where hydrogen dissociation does not show an enthalpy barrier, and the reaction is limited by the C−H bond formation.[13,23] Another distinctive feature is the rather weak 1-hexyne adsorption on $Pd_1Au(111)$, with an adsorption enthalpy of −1.16 eV and a slightly endergonic nature in the considered temperature and pressure conditions. The adsorption on pure Pd catalysts, on the other hand, is much stronger, with ΔH being −2.33 eV on Pd(111). The selective hydrogenation product 1-hexene shows a similar adsorption enthalpy (−1.22 eV) as 1-hexyne on $Pd_1Au(111)$, while its adsorption on Pd(111) (−1.46 eV) is much weaker than that of 1-hexyne. This suggests that the process controlling

https://doi.org/10.1021/acscatal.2c03560
ACS Catal. 2022, 12, 13321−13333

selectivity is different on the dilute Pd alloy, compared to bulk Pd catalysts.

Further hydrogenation of 1-hexene to 1-hexyl, 2-hexyl, and hexane proceeds with a similar mechanism, although the reaction is much less exergonic, with a DFT-calculated reaction free energy of −1.07 eV in the conditions shown in Figure 3, versus −1.49 eV for 1-hexyne to 1-hexene (Table S1). Due to the smaller exothermicity of the reaction, the intermediates connecting the reactant and the product lie higher in free energy in the case of 1-hexene hydrogenation. Hence, they encounter barriers of similar magnitude in both the forward and reverse direction, and the hydrogenation reaction of 1-hexene is reversible (Table S1). For completeness, a possible side reaction from the monohydrogenated 1-hexyne intermediate RHCCH has also been considered by hydrogenating the C_2 atom again to form RH_2CCH (1-hexylidene), followed by hydrogenation of C_1 to form 1-hexyl (Figure S2). That path would be detrimental to the selectivity of the alloy catalyst because it skips the formation of the desired 1-hexene and produces hexyls directly. However, it presents an overall free energy barrier of 1.09 eV on $Pd_1Au(111)$ under the considered conditions, which is at least 0.26 eV higher than that of the pathway to form 1-hexyl via 1-hexene. Hence, this pathway is energetically unfavorable and is unlikely to affect the selectivity for 1-hexene formation.

Experimental Verification of Irreversible H Addition to 1-Hexyne. The irreversibility of 1-hexyne partial hydrogenation to form 1-hexene was verified experimentally by running the reaction in D_2 over a dilute Pd-in-Au nanoparticle catalyst, where the absence of significant HD and 1-hexyne d_1 formation would confirm the expected irreversibility (Figure S4). The catalyst used was the so-called raspberry colloid-templated material (RCT) containing 4.9 ± 0.9 nm nanoparticles with 4 atm % Pd supported on a macroporous silica support (4.2 wt % total metal loading). For comparison, a monometallic $Pd_{100}Au_0$ on RCT-SiO_2 catalyst (6.9 ± 2.1 nm nanoparticles, 0.6 wt % total metal loading) was also tested. The catalytic performance of this Pd_4Au_{96} and $Pd_{100}Au_0$ on RCT-SiO_2 was probed under steady-state conditions in H_2 and D_2 (Figure S5) and at low conversion to ensure that 1-hexene is the only product formed and no HD formation is caused by the isomerization reaction between 1-hexene and 2-/3-hexene.

The experimental data (Figure 4) indicate that the addition of the H- or D-atoms to 1-hexyne is indeed irreversible over both the Pd_4Au_{96} and $Pd_{100}Au_0$ on SiO_2 catalysts. 1-Hexyne conversion is shown to decrease significantly when switching from H_2 and D_2 (Figure 4a,b). The conversion levels dropped from 10.6 to 4.6% and from 12.2 to 6.5% for the Pd_4Au_{96} and $Pd_{100}Au_0$ on RCT-SiO_2, respectively. This isotope effect is in clear agreement with the DFT result that H_2/D_2 dissociation is the rate-limiting process. No significant increase in HD/D_2 and 1-hexyne (m/z = 68, d_1)/1-hexyne (m/z = 67, d_0) ratios was measured between the bypass and the reactor values (Figure 4c,d). These findings are all consistent with irreversible H addition to the C≡C triple bond in 1-hexyne and therefore support the high barrier for the reverse process computed by DFT.

Microkinetic Simulation of Catalytic Activity. Microkinetic simulations were used to determine the factors that control the activity and selectivity of the reaction as a function of temperature. The details of the model are summarized in the Supporting Information (Table S2). Briefly, the microkinetic simulations were parameterized using kinetic rate constants

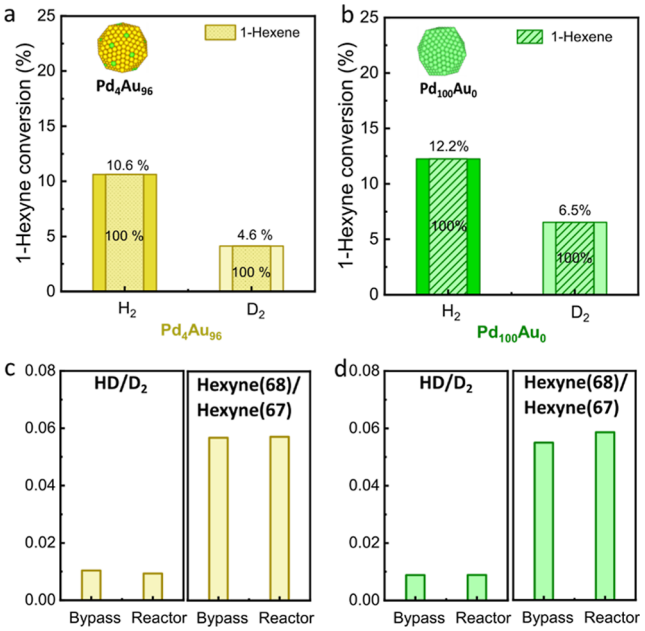

Figure 4. Experimental results showing the irreversibility of 1-hexyne hydrogenation on the Pd_4Au_{96} and $Pd_{100}Au_0$ catalysts. (a) 1-Hexyne conversion (values shown on top of the bars) and 1-hexene selectivity (values shown within the bars) for the Pd_4Au_{96} catalyst and (b) for the $Pd_{100}Au_0$ catalyst in H_2 and D_2. (c) HD/D_2 and 1-hexyne (m/z = 68, d_1)/1-hexyne (m/z = 67, d_0) ratios over the bypass and reactor for the Pd_4Au_{96} and (d) for the $Pd_{100}Au_0$ catalysts in D_2. The catalytic data were measured under steady-state conditions at 403 K (Pd_4Au_{96}) and 305 K ($Pd_{100}Au_0$) in 1% 1-hexyne, 20% H_2 or D_2 in Ar, with a total flow of 50 mL/min using a catalyst bed of 20 mg 4.2 wt % Pd_4Au_{96} and 10 mg 0.6 wt % $Pd_{100}Au_0$.

derived from the DFT energetics presented above. The adsorption rate constants of molecular H_2, 1-hexyne, 1-hexene, and *n*-hexane were computed using the kinetic theory of gases, while the desorption rate constants were computed as the ratio between the adsorption rate constant and the equilibrium constant of adsorption.

In the reaction mechanism, the hydrogenation of carbonaceous intermediates was assumed to only take place on $Pd_1Au(111)$ after H exchange between $Pd_1Au(111)$ sites across the Au substrate. Microkinetic simulations demonstrate that $Pd_1Au(111)$ is selective for 1-hexene formation at both low and high conversions. The rate-limiting step of the hydrogenation is found to be the dissociation of H_2, which is consistent with the free-energy-based analysis and contrasts with nanoparticle Pd catalysts. The kinetic orders of the reactants (1 for hydrogen and ∼0 for 1-hexyne) and the apparent activation energy are also in close agreement with the experimental results.[8]

The rate of 1-hexyne hydrogenation was evaluated under a typical experimental reaction environment at low conversion [T = 313−413 K, $P(H_2)$ = 0.2 bar, P(1-hexyne) = 0.01 bar, P(1-hexene) = P(*n*-hexane) = 0.001 bar]. 1-Hexyne starts to react at 333 K. At 373 K, the rate of selective hydrogenation to 1-hexene is 0.42 s^{-1}, while the rate of complete hydrogenation to *n*-hexane is 0.0021 s^{-1} (Figure 5a). Overall, in the temperature range of T = 313−413 K and low 1-hexyne conversion, the selectivity for the formation of 1-hexene was found to be consistently above 98%. The $Pd_1Au(111)$ active sites were found to be largely covered by adsorbed 1-hexyne and 1-hexene below 353 K but become mostly bare above this

https://doi.org/10.1021/acscatal.2c03560
ACS Catal. 2022, 12, 13321−13333

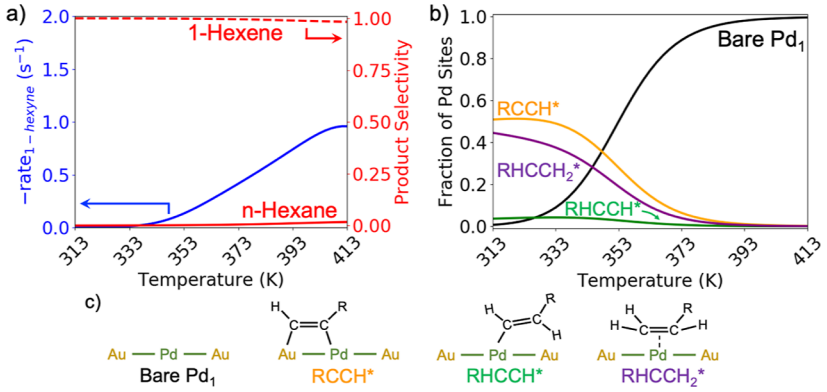

Figure 5. Microkinetic simulations of 1-hexyne hydrogenation to 1-hexene and *n*-hexane under a typical experimental reaction environment corresponding to low (<20%) conversion: $P(H_2)$ = 0.2 bar, P(1-hexyne) = 0.01 bar, P(1-hexene) = P(*n*-hexane) = 0.001 bar. (a) rate (s^{-1}) for the conversion of 1-hexyne (blue line) and selectivity for the formation of 1-hexene and *n*-hexane (red lines) as a function of temperature. The selectivity for 1-hexene was found to be above 98% through the temperature range T = 313−413 K. (b) Steady-state fraction of reactive intermediates on $Pd_1Au(111)$ as a function of temperature: adsorbed 1-hexyne (orange line) and 1-hexene (purple line) were found to be the most abundant reactive intermediates until 353 K. (c) Schematics of structures in panel (b).

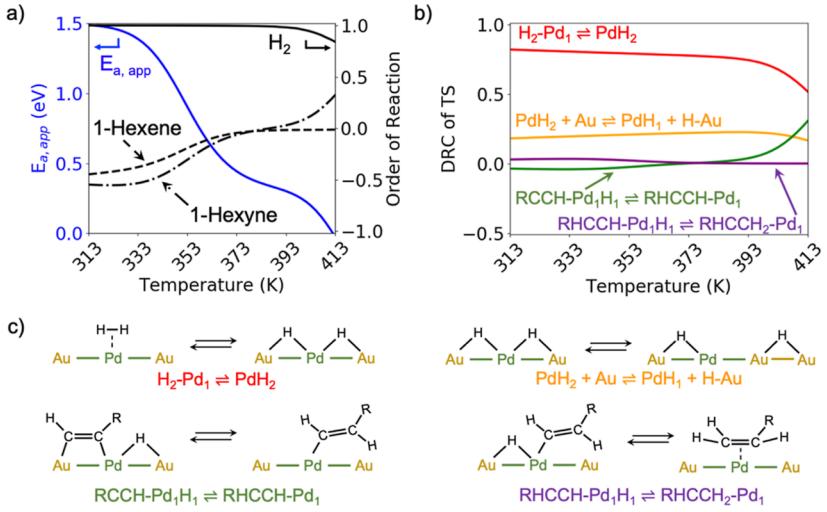

Figure 6. Analysis of the kinetics for hydrogenation of 1-hexyne shows H_2 dissociation to be the rate-controlling step. (a) Apparent activation enthalpy (blue line) and kinetic orders of H_2 (black solid line), 1-hexyne (dot-dashed line), and 1-hexene (dashed line) for the hydrogenation of 1-hexyne as a function of temperature. The apparent activation enthalpy of the reaction progressively decreases in the temperature range T = 313−413 K, while the orders of 1-hexyne and 1-hexene increase. (b) Degree of rate control (DRC) of various transition states as a function of temperature. The transition state for H_2 dissociation is the main rate-controlling transition state (red line), while the migration of H from the Pd single atom to the Au substrate (orange line) is second in importance. Importantly, C−H bond formation steps (green and purple lines) do not appear to be rate-controlling. (c) Schematics of the four elementary steps shown in panel (b).

temperature (Figure 5b). At up to 90% 1-hexyne conversion, the selectivity of 1-hexene remains high (>70%), in agreement with experimental findings (Figure S6).[8]

For the formation of 1-hexene from 1-hexyne, the C_2 atom was found to be hydrogenated first, in agreement with the Gibbs free energy−based analysis (Figure S7a). The formation of 1-hexenyl and 1-hexene was exothermic and irreversible: the reversibility factor, defined as the ratio between the reverse and forward rates of an elementary step with a positive rate (r_{rev}/r_{fwd}), is below 10^{-4} on the whole considered temperature range.[26] On the other hand, the formation of 1-hexyl was found to be partially reversible in the temperature range, with a reversibility factor ranging from ∼1 at 313 K to 0.46 at 413 K. Moreover, the formation of the 1-hexylidene intermediate and then hexyl and hexane were found to be unfavorable at all temperatures (Figure S7b).

The apparent activation enthalpy and kinetic orders of H_2, 1-hexyne, and 1-hexene for the consumption of 1-hexyne were next computed. Here, under an H_2-rich reaction environment and low 1-hexyne conversion [$P(H_2)$ = 0.2 bar, P(1-Hexyne) = 0.01 bar, P(1-Hexene) = 0.001 bar] along the rise of temperature from 313 to 373 K, the apparent activation enthalpy for the hydrogenation of 1-hexyne was found to decrease from 1.49 to 0.44 eV; the orders of 1-hexyne and 1-hexene were found to increase from ∼ −0.5 to ∼0, and the order of H_2 was found to be roughly constant at 1 (Figure 6a). The lowering of apparent activation enthalpy and increase in the kinetic orders of 1-hexyne and 1-hexene accompany a sharp increase in the rate of 1-hexyne hydrogenation without compromising the selectivity (Figure 5). At a reaction temperature of 373 K, the apparent activation enthalpy, order of H_2, and order of 1-hexyne were found to be 0.44 eV, 1, and −0.04, respectively.

https://doi.org/10.1021/acscatal.2c03560
ACS Catal. 2022, 12, 13321−13333

The kinetics of the semihydrogenation of 1-hexyne catalyzed by dilute Pd-in-Au alloys have been studied by two groups of authors. For the gas phase hydrogenation of 1-hexyne to 1-hexene at 313 K, Luneau et al. found the rate of 1-hexyne hydrogenation over Pd_4Au_{96} nanoparticles supported on RCT-SiO_2 to depend largely on the partial pressure of H_2 (order of 0.94) but weakly on the partial pressure of 1-hexyne (order of −0.08).[8] The authors found the apparent activation enthalpy to be 0.39 eV between 303 and 343 K. Based on the similarity of the orders of H_2 and 1-hexyne over Pd_4Au_{96} (0.94 for H_2 and −0.08 for 1-hexyne) to those over pure Pd (0.99 for H_2 and −0.20 for 1-hexyne), the authors suggested that the rate-controlling step over Pd_4Au_{96} should be the hydrogenation of 1-hexenyl to 1-hexene.[8]

For the liquid phase hydrogenation of 1-hexyne to 1-hexene, Liu et al. observed similar orders of reaction as Luneau et al. At 298 K, the authors found the rate of reaction to have a linear dependence on the pressure of H_2 but no dependence on the concentration of 1-hexyne, corresponding to an order of ∼1 for H_2 but ∼0 for 1-hexyne.[24] In the temperature range of 273−318 K, the authors found the apparent activation enthalpy of the reaction to be 0.43 eV, and due to the similarity of this apparent activation enthalpy to that of the H/D exchange reaction [$H_2 + D_2 \rightarrow 2HD$, $E_{a,app}$ = 0.43 eV] over the same catalyst, they suggested that H_2 activation should be the rate-controlling step.[24]

At face value, the calculated apparent activation enthalpy and orders of reaction in this work agree with those measured by Luneau et al., but they are appearing at a higher temperature, shifted by ∼60 K. The origin of this shift will be discussed further later.

To determine the rate-limiting process and quantify the relative importance of surface intermediates and transition states, a degree of rate control (DRC) analysis was performed on the rate of 1-hexyne hydrogenation (Figures 6b and S8).[27] In the temperature range T = 313−353 K, the most abundant surface intermediates are adsorbed 1-hexyne and 1-hexene, but more than half the Pd sites become bare above 353 K (Figure 5b). This depletion of the surface C_6 intermediates is mirrored in the calculated DRCs of reactive intermediates, where the DRCs of surface intermediates gradually move to 0 in this temperature range, while the bare surface becomes the rate-controlling intermediate (Figure S8). The loss of surface C_6 intermediates accompanies both the decrease of apparent activation enthalpy and the increase of C_6 reaction orders in this temperature range. On the other hand, the dissociation of H_2 remains the main rate-controlling transition state for the reaction on the whole temperature range. The calculated apparent activation enthalpy and reaction orders can be rationalized through the DRCs. Following Mao and Campbell, the apparent activation enthalpy can be interpreted as approximately the difference between the enthalpic barrier for H_2 dissociation relative to H_2 gas and the enthalpies of adsorption of 1-hexyne and 1-hexene weighed by the DRCs of their adsorbed states.[28] Through these analyses, the transition state for the dissociation of H_2 was shown to be the main rate-controlling step for the hydrogenation of 1-hexyne to 1-hexene, in agreement with the qualitative analysis from reaction pathways.

$$r = \frac{K_1 k_{2f} P_{H_2} \theta_{Pd,0}}{1 + K_5 P_{1-HY} + K_{10} P_{1-HE}} \quad (1)$$

Rate laws derived by assuming the existence of a single rate-controlling transition state show that two cases yield a rate law that is first-order in H_2 and zero-order in 1-Hexyne: H_2 dissociation or hydrogenation of 1-hexenyl to 1-hexene (Table S3). In these derivations, the transition states of H_2 dissociation, hydrogenation of adsorbed 1-hexyne to 1-hexenyl, or hydrogenation of 1-hexenyl to 1-hexene could be the rate-controlling steps. Comparing the formulated rate laws to the measured orders of reaction,[8,24] the hydrogenation of 1-hexyne to 1-hexenyl can be immediately ruled out as the possible rate-limiting step because its rate law will always be one half-order in H_2. On the other hand, the H_2 dissociation-limited rate law (eq 1) best fits the results of the microkinetic simulations and the reported kinetic studies.[8,24] Under a reaction environment where the coverage of surface C_6 intermediates is low, the rate law indicates that the rate of 1-hexene formation is solely dependent on the partial pressure (or activity) of H_2. At this limit, the apparent activation energy is simply equal to the enthalpy barrier for dissociating H_2 over the Pd_1 site. The microkinetic model agrees well with the derived rate law. At T = 393 K and low 1-hexyne conversion [$P(H_2)$ = 0.2 bar, P(1-hexyne) = 0.01 bar, P(1-hexene) = P(*n*-hexane) = 0.001 bar], the apparent activation energy was found to be 0.30 eV (Figure 6), very close to the 0.29 eV enthalpy barrier to dissociate H_2 gas over Pd_1 at this temperature.

From the derived rate laws, it also seems possible that the transition state of 1-hexenyl hydrogenation to 1-hexene is the rate-controlling step, if adsorbed 1-hexyne was the most abundant surface intermediate. However, this is unlikely due to two reasons. First, based on the temperature-programmed desorption (TPD) experiments of Liu et al. and on gas phase chemical potential calculations, the adsorption of 1-hexyne on Pd sites must be endergonic (Figure S9), resulting in very low coverage of 1-hexyne under typical reaction temperatures.[24] Second, the requirement for 1-hexenyl hydrogenation to be the rate-controlling step and for 1-hexyne to be the most abundant surface intermediate imposes a thermodynamically inconsistent constraint on the reaction network. The Gibbs free energy barrier of H_2 dissociation over $Pd_1Au(111)$ was found to be 0.86 eV at 363 K and $P(H_2)$ = 0.2 bar (Figure 2). Following the Brønsted−Evans−Polanyi relation for the C−H bond formation reactions studied in this work (Figure S10), the hydrogenation of 1-hexenyl by co-adsorbed H must be highly endothermic ($\Delta E \gg 0$ eV) to overtake the H_2 dissociation barrier and become the rate-controlling step. Assuming 1-hexyne and 1-hexene have similar adsorption energies, the hydrogenation of adsorbed 1-hexyne by co-adsorbed H to 1-hexenyl then must be extremely exothermic ($\Delta E \ll -2$ eV) to ensure thermodynamic consistency of the gas phase reaction. The consequentially exothermic hydrogenation of 1-hexyne to 1-hexenyl must have a very small forward activation energy. In total, the thermodynamic constraint would make 1-hexenyl the most abundant surface intermediate, contradicting the previous assumption, where 1-hexyne is the most abundant surface intermediate. Based on these reasons, the hydrogenation of 1-hexenyl can be ruled out as the rate-controlling step, further strengthening the proposal that the dissociation of H_2 is the rate-controlling step for the reaction.

One possible origin of the difference between the microkinetic simulations and the kinetic experiments of Luneau et al. could be the calculated adsorption enthalpies of 1-hexyne and 1-hexene. In our calculations, the desorption enthalpies of 1-hexyne and 1-hexene were calculated to be 1.16 and 1.22 eV,

https://doi.org/10.1021/acscatal.2c03560
ACS Catal. 2022, 12, 13321−13333

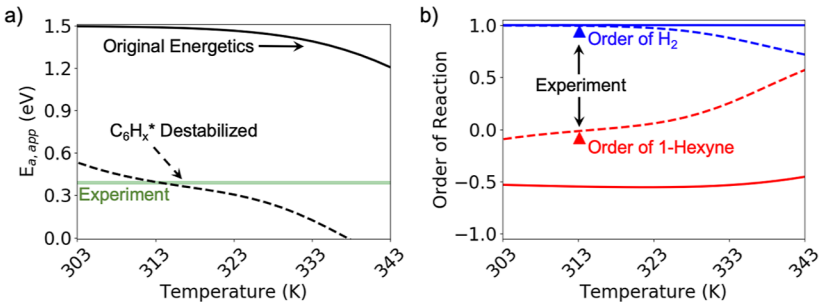

Figure 7. Destabilization of hydrocarbon intermediates and transition states energy by 0.2 eV enables an improved agreement with the experiment for the kinetic order of 1-hexyne and the apparent activation enthalpy. (a) Apparent activation enthalpy (eV) of 1-hexyne hydrogenation as a function of temperature without (full line) and with (dashed line) destabilization of surface C_6H_x intermediates and transition states. The experimental value (+0.39 eV, reported in ref 8) is shown as a green horizontal bar. (b) Orders of reaction of H_2 (blue) and 1-hexyne (red) as a function of temperature without (full line) and with (dashed line) destabilization of surface C_6H_x intermediates and transition states. Experimental values (order of H_2: 0.94, order of 1-hexyne: −0.08, reported in ref 8) are shown as triangles.

respectively, at 363 K. The values appear overestimated compared to the TPD experiments of Liu et al.[24] Compared to the gas phase chemical potentials of 1-hexyne and 1-hexene (Figure S9), the overestimation of the desorption enthalpies would result in higher calculated coverage of C_6 intermediates at typical reaction temperatures, 298−343 K.

To qualitatively reconcile the differences, a modified microkinetic model was created, where surface intermediate states and transition states containing adsorbed carbonaceous species were destabilized by 0.20 eV (Figure 7). At 313 K, the apparent activation enthalpy was found to be 0.39 eV, and the order of 1-hexyne was −0.01. The calculated apparent activation enthalpy and orders of reaction from this modified model compare much more favorably with the experimental measurements by Luneau et al. (apparent activation enthalpy: +0.39 eV, order of 1-hexyne: −0.08) and Liu et al. (apparent activation enthalpy: +0.43 eV, order of 1-hexyne: ∼0), while the dissociation of H_2 remains as the main rate-controlling transition state.

Origin of Improved 1-Hexene Selectivity. The degree of selectivity controls (DSC)[27] of all surface intermediates and transition states were computed at a typical low-conversion experimental reaction environment [T = 373. K, $P(H_2)$ = 0.2 bar, P(1-hexyne) = 0.01 bar, P(1-hexene) = 0.001 bar] to quantitatively compare the influence of the elementary steps in the reaction network on 1-hexene selectivity. The DSCs of the transition states for H_2 dissociation on Pd_1 and for 1-hexyl hydrogenation to form *n*-hexane are negative (Figure 8), meaning that the selectivity for 1-hexene formation is decreased if the free energy of the TS for H_2 dissociation or 1-hexyl hydrogenation is lowered. The former is justified by the fact that atomic H would become more readily available for 1-hexene hydrogenation when the H_2 dissociation barrier shrinks. The latter is even more natural, as it directly controls the formation of the undesired *n*-hexane product. The calculated DSCs agree well with the Gibbs free energy-based analysis. On the other hand, the transition state with the largest positive DSC goes to the hydrogenation of 1-hexyne to form 1-hexenyl (Figure 8). Since the first hydrogenation step of 1-hexyne has a larger activation barrier than the second step, lowering this TS free energy could more significantly increase the yield of 1-hexene and hence the selectivity. It is noted that the DSC analysis is carried out at a condition under which only 11% of all surface Pd sites are occupied by carbonaceous

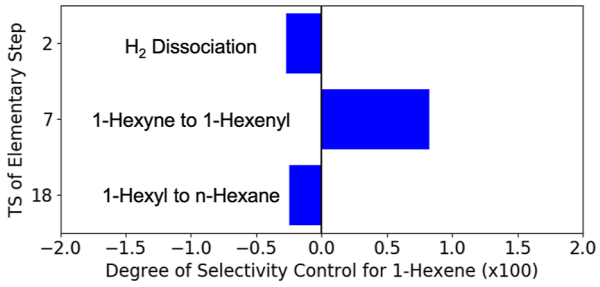

Figure 8. Degree of selectivity control (DSC), evaluated at T = 373 K, $P(H_2)$ = 0.2 bar, P(1-hexyne) = 0.01 bar, P(1-hexene) = 0.001 bar, of the TS for H_2 dissociation over Pd_1 (DSC = -2.75×10^{-3}), 1-hexyne hydrogenation to 1-hexenyl (DSC = 8.24×10^{-3}), and 1-hexyl hydrogenation to *n*-hexane (DSC = -2.46×10^{-3}). The values were multiplied by 100 in the figure. Decreasing the free energy barrier for 1-hexyne hydrogenation to 1-hexenyl increases the selectivity for 1-hexene, while decreasing the free energy barrier of H_2 dissociation and 1-hexyl hydrogenation to *n*-hexane decreases the selectivity for 1-hexene.

intermediates; thus, the influence of site-competition is negligible (Figure 5b).

At low conversion, Pd catalysts achieve high selectivity via competitive binding: strong binding of 1-hexyne expels the relatively weakly bound 1-hexene from the catalyst surface. This competitive binding, however, would be lost when conversion becomes higher. The high selectivity of the dilute Pd-in-Au catalyst at high conversion, on the other hand, does not rely on competitive binding, as can be seen from the similar magnitude of adsorption energies of 1-hexyne and 1-hexene. Instead, the selectivity is mainly controlled by the difference in the hydrogenation rates constants between 1-hexyne and 1-hexyl, as shown by the DSC analysis. One important factor to slow down 1-hexyl hydrogenations is the high H_2 dissociation barrier, which encourages hexyls to proceed in the reverse direction to form hexenes, as also demonstrated by van der Hoeven et al. in the case of hexene hydrogenation on the same catalyst.[29] Notably, this sizable barrier is absent on the Pd catalysts.[13] Since the H_2 dissociation barrier is independent of reaction conversion, the selectivity for hexene formation can be preserved even at high conversion. The production of hexyls via hexylidene, which is detrimental to the selectivity as it skips the formation of 1-hexene, is also energetically unfavorable on the alloy

https://doi.org/10.1021/acscatal.2c03560
ACS Catal. 2022, 12, 13321−13333

catalyst (Figure S2). All these features together contribute to the much improved selectivity of the $Pd_1Au(111)$ catalyst.

One can discuss in more detail the differences between the $Pd_1Au(111)$ and bulk Pd(111) catalysts for 1-hexyne hydrogenation. The hydrogenation energy profiles differ in that the surface intermediates and transition states are much more weakly adsorbed on $Pd_1Au(111)$. Compared to Pd(111), adsorbed 1-hexyne is destabilized in free energy by 1.37 eV on $Pd_1Au(111)$, and the first C−H bond formation TS1(a) by a similar amount of 1.33 eV (Figure S3). Hydrogen adsorption is weaker as well, destabilized by 0.49 eV/H atom.[30] The co-adsorbed state, where both 1-hexyne and H are interacting with Pd_1, is destabilized by 1.87 eV and hence roughly cumulates the two effects. As a result, for the elementary C−H bond formation process, the reactant state is more destabilized than the TS, leading to the activation energy being reduced from 0.86 eV on Pd(111) to 0.32 eV on $Pd_1Au(111)$. The observed destabilizations on the single atom alloy[8,31−33] mainly stem from reduced active ensemble effects, for example, on Pd(111), 1-hexyne binds to three Pd atoms, while it binds to one Pd and two Au atoms on $Pd_1Au(111)$. The d states of Au are lower in energy, completely occupied, and cannot interact strongly with the adsorbate.[34] Electronic effects are also present since the electronic states on Pd for the single-atom alloy are less dispersed in energy than for a surface atom of Pd(111).[35] Note, however, that the d band center for the surface Pd atom has a very similar value [−1.69 eV for Pd(111) and −1.65 eV for $Pd_1Au(111)$, Figure S11], so that electronic effects should remain moderate. The marked destabilization along the energy profile results in large H_2 dissociation activation energy and small C−H bond formation activation energy on $Pd_1Au(111)$, with strong positive consequences on the 1-hexyne hydrogenation selectivity, as shown from our kinetic analysis. Since ensemble effects dominate, one can expect that the phenomenon shown here would reasonably pertain to a wide range of single-atom alloys.

The concepts obtained in this study can be used to design selective catalysts. One important parameter is the energy barrier for H_2 dissociation, for which we face a compromise between activity and selectivity. Increasing further the H_2 dissociation barrier would decrease the activity (it is the main rate-controlling process), while decreasing it significantly could damage the selectivity. We can play, however, in an interval of favorable barrier values to find an optimal situation. This can be done by keeping Pd as active metal but changing the host to Ag or Cu.[32] One other possibility is to change the active metal to Ni. Changing the active metal to Pt does not appear to be a good idea, since the H_2 dissociation barrier is much smaller on Pt SAAs in Au, Ag, and Cu.[32] Larger ensembles of Pd or Ni as dimers or trimers would also markedly decrease the H_2 dissociation barrier, at the expense of selectivity, and should not be an efficient direction of design.

CONCLUSIONS

In this work, our combined theoretical and experimental study shows that over dilute Pd-in-Au alloy catalysts, the H_2 dissociation elementary step, with a sizable free energy barrier of 0.86 eV at 363 K and 0.2 bar of H_2, plays a major role in controlling the activity and selectivity of 1-hexyne hydrogenation. Specifically, our Gibbs free energy-based analysis and first-principles microkinetic simulations show that H_2 dissociation is the rate-limiting process for 1-hexyne hydrogenation on $Pd_1Au(111)$, while the C−H bond formation steps proceed with lower barriers. Somewhat more surprisingly, the sizable H_2 dissociation barrier also favorably impacts the selectivity for partial hydrogenation to 1-hexene because it slows down the undesired overhydrogenation to hexane. This is shown by our DSC analysis, which indicates that decreasing the free energy barrier of H_2 dissociation decreases the selectivity for 1-hexene. Other elementary steps are also important for the selectivity: decreasing the barrier for 1-hexyl hydrogenation to *n*-hexane also decreases the selectivity for 1-hexene, while decreasing the barrier for 1-hexyne hydrogenation to 1-hexenyl increases it.

This major role of H_2 dissociation in the kinetic control of 1-hexyne hydrogenation on dilute Pd-in-Au catalysts markedly contrasts with previously studied extended Pd catalysts, for which the addition of atomic H to the adsorbed alkyne or alkenyl is accepted to be the rate-determining step, and the selectivity is controlled by competitive adsorption of alkyne and alkene. On dilute Pd-in-Au, the selectivity is controlled instead by competition of hydrogenation rates of alkyne and alkene, which maintains a high selectivity even at high conversion. Hence, the energetics and kinetics of the 1-hexyne hydrogenation mechanism over dilute Pd-in-Au alloy are distinct with respect to bulk Pd catalysts. Our reaction profiles from first-principles calculations and microkinetic modeling also reveal that 1-hexyne hydrogenation to 1-hexene is an irreversible process due to the strongly exothermic nature of the reaction. This claim is validated through the isotopic exchange hydrogenation experiment conducted on $Pd_{0.04}Au_{0.96}$ embedded in RCT-SiO_2.

Another key property of dilute Pd-in-Au alloys is that the adsorption energy of hydrocarbon species is moderate, so that the coverage of Pd sites by these hydrocarbon intermediates is low, enabling access and activation of H_2 and preventing poisoning and coking of the catalysts. This is again different from extended Pd catalysts, where hydrocarbon species bind strongly and can form coke at high coverage, deactivating the catalyst. Apparent activation enthalpies and reaction orders for dilute Pd-in-Au from our microkinetic modeling are in good agreement with previous experiments despite a shift of ∼60 K in temperature. The temperature shift is attributed to the slight overestimation of the adsorption energies of the surface species when the xc-functional optPBE-vdW is used. Altogether, this work unprecedentedly demonstrates that the improved selectivity of the dilute Pd-in-Au alloy catalyst is attributed to the sizable H_2 dissociation barrier and the small barrier for C−H bond formation from 1-hexyne to 1-hexenyl (smaller than that for C−H bond formation from 1-hexene to 1-hexyl). The formation of dilute active species in a less active host metal can therefore be seen as a way to tune the binding energy of reactants, alter reaction profiles, and induce distinct kinetic behaviors for an optimal catalytic activity and selectivity. This concept of dilute alloy catalyst is hence a versatile approach to design highly selective heterogeneous catalysts.

METHODS

Computational Details. *DFT Calculations.* All DFT calculations were performed using the Vienna ab initio simulation package (VASP).[36,37] A six-layer slab and a (4 × 4) unit cell were employed to model the $Pd_1Au(111)$ surface for 1-hexyne hydrogenation. It was constructed by replacing one surface Au atom of Au(111) with a single Pd atom. Adsorption energies of a single H atom calculated using different exchange−correlation functionals were benchmarked

https://doi.org/10.1021/acscatal.2c03560
ACS Catal. 2022, 12, 13321−13333

against the low energy recoil scattering and nuclear microanalysis experiments, and optPBE-vdW[38−40] was shown to be in closest agreement.[41−43] In addition, various density functionals were benchmarked by comparing their calculated adsorption energy of 1-hexyne to that obtained from TPD (Supporting Section 8); the optPBE-vdW functional was also found to perform the best. Thus, only computations performed using this functional were reported. A plane wave basis set with a cutoff energy of 400 eV and a Monkhorst-Pack[44] generated 7 × 7 × 1 *K*-points grid were used for all calculations. The second-order Methfessel-Paxton smearing method with the width of smearing set to 0.2 eV was also utilized.[45] During optimization, the bottom four atomic layers were fixed in the Au bulk position while the upper two layers and the adsorbates were allowed to relax until the convergence threshold of <0.03 eV/Å was reached. Transition states were fully optimized using the dimer method[46] and the quasi-Newton method. All atomic structures reported in this study are visualized using VESTA.[47]

For simplicity, only the translational and rotational entropies of the gaseous species were considered in the free energy calculations. Zero-point energies (ZPEs) and vibrational entropies were neglected for all species. The ZPEs of gaseous H_2 and the most rate-controlling transition state (H_2 dissociation) are both 0.27 eV.[48] The H−H stretch mode has no ZPE contribution in the transition state, but five H-surface vibrational modes appear and their ZPE contributions sum up to 0.27 eV as well. Hence, the difference in the ZPEs is small for the rate-controlling process, and the neglect of ZPE would not affect the overall reaction kinetics.

Microkinetic Simulations. Microkinetic simulations to quantitatively compare the theoretically proposed reaction pathway to the experimental measurements. The kinetic rate parameters were computed from DFT energetics. The forward and reverse rate constants of surface reactions were computed using transition state theory:

$$k_i = \frac{k_B T}{h} \exp\left(\frac{-\Delta G^\circ_{act}}{RT}\right)$$

The rate constants for the adsorption of gas molecules were computed with collision theory for adsorption and desorption steps[49]

$$k_{ads,\,i} = \frac{\sigma A_{site} P^\circ}{\sqrt{2\pi m_i k_B T}}$$

where σ is the sticking coefficient, A_{site} is the area of the active site, P° is the standard state pressure, m_i is the mass of the adsorbate, and k_B is Boltzmann's constant. Here, the sticking coefficient was assumed to be 1. The surface area of an active site was calculated using the experimental bulk lattice constants of Pd and Au (3.88 and 4.06 Å, respectively). The atomic fraction of Pd in the alloy is set to 5%. Following Vegard's law, the area occupied by one atom on (111) facet is 7.10×10^{-20} m^2. The corresponding rate constants of desorption were computed using the equilibrium constants of adsorption:

$$k_{des,i} = \frac{k_{ads,i}}{K_{ads,i}}$$

$$K_{ads,i} = \exp\left(-\frac{\Delta G^\circ_{ads,i}}{k_B T}\right)$$

The rate of elementary step j was computed using the following equation:

$$r_j = k_j^{fwd} \prod_i \alpha_{i,IS}^{\nu_{ij}^{fwd}} \prod_i \alpha_{i,gas}^{\nu_{ij}^{fwd}} - k_j^{rev} \prod_i \alpha_{i,IS}^{\nu_{ij}^{rev}} \prod_i \alpha_{i,gas}^{\nu_{ij}^{rev}}$$

where k_j^{fwd} and k_j^{rev} are the forward and reverse rate constants, and ν_{ij}^{fwd} and ν_{ij}^{rev} are the stoichiometric coefficients of reactant i in the forward and reverse directions, respectively. The activity α_i was assumed to be the surface coverage fraction θ_i for surface intermediates (including bare sites) and as the ratio of the partial pressure to the standard pressure, P_i/P°, for gaseous species.[50]

The time-dependent coverages of surface intermediates are obtained as the steady-state solution of the following system of ordinary differential equations:

$$\frac{d\theta_i}{dt} = -\sum_j \nu_{ij}^{fwd} r_j + \sum_j \nu_{ij}^{rev} r_j$$

Following Wang et al., the steady-state solution is achieved in two steps.[51] Starting from a bare surface, the equations are first integrated over 500 s until they have approximately reached a steady state. The resulting coverages are then used as an initial guess for the numerical solution as follows:

$$0 = -\sum_j \nu_{ij}^{fwd} r_j + \sum_j \nu_{ij}^{rev} r_j$$

$$\theta_{Pd}(t=0) = \sum_i \theta_{Pd,i},$$

$$1 = \sum_i \theta_{Pd,i} + \sum_i \theta_{Au,\,i}.$$

where $\theta_{Pd,i}$ and $\theta_{Au,i}$ are the surface coverages of species i on Pd and Au sites, respectively.

EXPERIMENTAL SECTION

The synthesis of the Pd_4Au_{96} and $Pd_{100}Au_0$ RCT catalysts is described by van der Hoeven et al.[25]

Prior to catalysis, the RCT catalysts were sieved (100−300 μm). For the Pd_0Au_{100} and Pd_4Au_{96}, RCT catalysts of 10 and 20 mg, respectively, were loaded into a cylindrical quartz reactor tube with an inner diameter of 1 cm. The catalysts were diluted in quartz sand to obtain a 1 cm bed height. Pretreatment in 20% O_2 in Ar at a flow rate of 50 mL/min was done to segregate Pd to the NP surface of the Pd_4Au_{96} nanoparticles.[52] In short, the catalysts were heated to 500 °C with 10 K/min and kept at 773 K for 30 min, followed by cooling in 40 mL/min Ar to 373 K. From 373 K to RT, the catalysts were cooled in 20% H_2 in Ar to ensure reduction of the Pd atoms. The reaction mixture was premixed on bypass for at least 2 h prior to the start of the experiment. In the steady-state 1-hexyne hydrogenation experiments, the reaction mixture was composed of 1% 1-hexyne, 20% H_2, or 20% D_2 in Ar with a total flow rate of 50 mL/min. The 1-hexyne flow was achieved by evaporating 1-hexyne using a 3.8 mL/min Ar flow at room temperature (yielding a 1-hexyne flow of 0.5 mL/min).

The reaction products were analyzed using both an online mass spectrometer (Hiden HAL 301/3F Series) and an online gas chromatography−mass spectrometer (Agilent 7890A series GC, Agilent 5975C series MS). The separate mass spectrometer was used to monitor m/z = 2, 3, 4, 40, 67, and

https://doi.org/10.1021/acscatal.2c03560
ACS Catal. 2022, 12, 13321−13333

68 corresponding to H_2, HD, D_2, Ar, 1-hexyne(d_0), and 1-hexyne(d_1), respectively. The inlet pressure for the MS was set at 9×10^{-7} torr and the scan rate was typically 0.1−1 channel/s. The sensitivity of the MS for each m/z value was set between −7 and −10, depending on the concentration of each component in the reaction mixture. The GCMS was used to quantify the amount of 1-hexyne and 1-hexene, and the number of deuterium atoms they contained.

Quantitative Mass Spectrometry Analysis and Gas Chromatography Mass Spectrometry Analysis. The mass spectrometer data were used to quantify the HD (m/z = 3) to D_2 (m/z = 4) ratio, and the 1-hexyne d_1 (m/z = 68) to 1-hexyne d_0 (m/z = 67) ratio on bypass and over the reactor in D_2. Additionally, the 1-hexyne d_0 signal (m/z = 67) was used to 1-hexyne compute the conversion in H_2 and D_2, by calculating the difference in signal intensity over the reactor compared to the signal over the bypass. These conversion levels were verified by also calculating the 1-hexyne conversion based on the GCMS data, using the following formula:

$$\text{Conversion}(\%) = \frac{\frac{A_{\text{Hexene}}}{\sigma_{\text{Hexene}}}}{\frac{A_{\text{Hexyne}}}{\sigma_{\text{Hexyne}}} + \frac{A_{\text{Hexene}}}{\sigma_{\text{Hexene}}}} \times 100\%$$

where A is the area under the peak for 1-hexene and 1-hexyne peaks in the gas chromatogram and σ is the ionization cross-section, for which 14.8 and 16.3 were taken for 1-hexyne and 1-hexene, respectively.[53] The number of deuterium atoms incorporated in 1-hexene was analyzed by quantifying the GC chromatograms with m/z = 84, 85, 86, 87, and 88.

■ ASSOCIATED CONTENT

Supporting Information

The Supporting Information is available free of charge at https://pubs.acs.org/doi/10.1021/acscatal.2c03560.

Adsorption configurations, additional microkinetic simulation analysis and experimental reactor studies, DFT functional performance, and computed electronic structures of metal catalysts (PDF)

■ AUTHOR INFORMATION

Corresponding Authors

Cynthia M. Friend − *Department of Chemistry and Chemical Biology, Harvard University, Cambridge, Massachusetts 02138, United States; Harvard John A. Paulson School of Engineering and Applied Sciences, Harvard University, Cambridge, Massachusetts 02138, United States;* orcid.org/0000-0002-8673-9046; Email: friend@fas.harvard.edu

Philippe Sautet − *Department of Chemical and Biomolecular Engineering and Department of Chemistry and Biochemistry, University of California, Los Angeles, California 90095, United States;* orcid.org/0000-0002-8444-3348; Email: sautet@ucla.edu

Authors

Hio Tong Ngan − *Department of Chemical and Biomolecular Engineering, University of California, Los Angeles, California 90095, United States*

George Yan − *Department of Chemical and Biomolecular Engineering, University of California, Los Angeles, California 90095, United States*

Jessi E. S. van der Hoeven − *Department of Chemistry and Chemical Biology, Harvard University, Cambridge, Massachusetts 02138, United States; Harvard John A. Paulson School of Engineering and Applied Sciences, Harvard University, Cambridge, Massachusetts 02138, United States; Materials Chemistry and Catalysis, Debye Institute for Nanomaterials Science, Utrecht University, 3584 CG Utrecht, The Netherlands;* orcid.org/0000-0001-9832-289X

Robert J. Madix − *Harvard John A. Paulson School of Engineering and Applied Sciences, Harvard University, Cambridge, Massachusetts 02138, United States;* orcid.org/0000-0002-3132-2382

Complete contact information is available at: https://pubs.acs.org/10.1021/acscatal.2c03560

Author Contributions

P.S., C.M.F., and R.J.M. guided the research. H.T.N. performed the DFT calculations, advised by P.S. G.Y. performed the microkinetic modeling. J.v.d.H. prepared the catalysts and conducted the catalysis experiments. All authors participated in discussions and have approved the final version of the manuscript.

Notes

The authors declare no competing financial interest.

■ ACKNOWLEDGMENTS

This work was supported as part of the Integrated Mesoscale Architectures for Sustainable Catalysis (IMASC), an Energy Frontier Research Center funded by the U.S. Department of Energy, Office of Science, Basic Energy Sciences under Award # DE-SC0012573. The DFT calculations in this work used computational and storage services associated with the Hoffman2 cluster at the UCLA Institute for Digital Research and Education (IDRE), the National Energy Research Scientific Computing Center (NERSC) of the U.S. Department of Energy, and the Bridges-2 cluster through the allocation TG-CHE170060 at the Pittsburgh Supercomputing Center (supported by National Science Foundation award number ACI-1928147) through the Extreme Science and Engineering Discovery Environment (supported by National Science Foundation grant number ACI-1548562).[54,55]

■ REFERENCES

(1) Zhang, L.; Zhou, M.; Wang, A.; Zhang, T. Selective Hydrogenation over Supported Metal Catalysts: From Nanoparticles to Single Atoms. *Chem. Rev.* **2020**, *120*, 683−733.

(2) Cárdenas-Lizana, F.; Keane, M. A. The Development of Gold Catalysts for Use in Hydrogenation Reactions. *J. Mater. Sci.* **2013**, *48*, 543−564.

(3) Lindlar, H. Ein Neuer Katalysator Für Selektive Hydrierungen. *Helv. Chim. Acta* **1952**, *35*, 446−450.

(4) Schwab, F.; Weidler, N.; Lucas, M.; Claus, P. Highly Cis-Selective and Lead-Free Hydrogenation of 2-Hexyne by a Supported Pd Catalyst with an Ionic-Liquid Layer. *Chemical Communications* **2014**, *50*, 10406−10408.

(5) Studt, F.; Abild-Pedersen, F.; Bligaard, T.; Sorensen, R. Z.; Christensen, C. H.; Norskov, J. K. Identification of Non-Precious Metal Alloy Catalysts for Selective Hydrogenation of Acetylene. *Science* **19792008**, *320*, 1320−1322.

(6) Sheth, P. A.; Neurock, M.; Smith, C. M. A First-Principles Analysis of Acetylene Hydrogenation over Pd(111). *J. Phys. Chem. B* **2003**, *107*, 2009−2017.

(7) Mei, D.; Sheth, P. A.; Neurock, M.; Smith, C. M. First-Principles-Based Kinetic Monte Carlo Simulation of the Selective Hydrogenation of Acetylene over Pd(111). *J. Catal.* **2006**, *242*, 1−15.
(8) Luneau, M.; Shirman, T.; Foucher, A. C.; Duanmu, K.; Verbart, D. M. A.; Sautet, P.; Stach, E. A.; Aizenberg, J.; Madix, R. J.; Friend, C. M. Achieving High Selectivity for Alkyne Hydrogenation at High Conversions with Compositionally Optimized PdAu Nanoparticle Catalysts in Raspberry Colloid-Templated SiO2. *ACS Catal.* **2020**, *10*, 441−450.
(9) Zaera, F. The Surface Chemistry of Metal-Based Hydrogenation Catalysis. *ACS Catal.* **2017**, *7*, 4947−4967.
(10) Han, J.; Lu, J.; Wang, M.; Wang, Y.; Wang, F. Single Atom Alloy Preparation and Applications in Heterogeneous Catalysis. *Chin. J. Chem.* **2019**, *37*, 977−988.
(11) Giannakakis, G.; Flytzani-Stephanopoulos, M.; Sykes, E. C. H. Single-Atom Alloys as a Reductionist Approach to the Rational Design of Heterogeneous Catalysts. *Acc. Chem. Res.* **2019**, *52*, 237−247.
(12) Darby, M. T.; Stamatakis, M.; Michaelides, A.; Sykes, E. C. H. Lonely Atoms with Special Gifts: Breaking Linear Scaling Relationships in Heterogeneous Catalysis with Single-Atom Alloys. *J. Phys. Chem. Lett.* **2018**, *9*, 5636−5646.
(13) Kyriakou, G.; Boucher, M. B.; Jewell, A. D.; Lewis, E. A.; Lawton, T. J.; Baber, A. E.; Tierney, H. L.; Flytzani-stephanopoulos, M.; Sykes, E. C. H. Isolated Metal Atom Geometries as a Strategy for Selective Heterogeneous Hydrogenations. *Science* **2012**, *335*, 1209−1213.
(14) Yuan, D.; Gong, X.; Wu, R. Atomic Configurations of Pd Atoms in PdAu(111) Bimetallic Surfaces Investigated Using the First-Principles Pseudopotential Plane Wave Approach. *Phys. Rev. B* **2007**, *75*, 085428.
(15) Thirumalai, H.; Kitchin, J. R. Investigating the Reactivity of Single Atom Alloys Using Density Functional Theory. *Top. Catal.* **2018**, *61*, 462−474.
(16) Greiner, M. T.; Jones, T. E.; Beeg, S.; Zwiener, L.; Scherzer, M.; Girgsdies, F.; Piccinin, S.; Armbrüster, M.; Knop-Gericke, A.; Schlögl, R. Free-Atom-like d States in Single-Atom Alloy Catalysts. *Nat. Chem.* **2018**, *10*, 1008−1015.
(17) Fung, V.; Hu, G.; Sumpter, B. Electronic Band Contraction Induced Low Temperature Methane Activation on Metal Alloys. *J Mater Chem A Mater* **2020**, *8*, 6057−6066.
(18) Vignola, E.; Steinmann, S. N.; Al Farra, A.; Vandegehuchte, B. D.; Curulla, D.; Sautet, P. Evaluating the Risk of C−C Bond Formation during Selective Hydrogenation of Acetylene on Palladium. *ACS Catal.* **2018**, *8*, 1662−1671.
(19) Liu, J.; Shan, J.; Lucci, F. R.; Cao, S.; Sykes, E. C. H.; Flytzani-Stephanopoulos, M. Palladium-Gold Single Atom Alloy Catalysts for Liquid Phase Selective Hydrogenation of 1-Hexyne. *Catal. Sci. Technol.* **2017**, *7*, 4276−4284.
(20) Boucher, M. B.; Zugic, B.; Cladaras, G.; Kammert, J.; Marcinkowski, M. D.; Lawton, T. J.; Sykes, E. C. H.; Flytzani-Stephanopoulos, M. Single Atom Alloy Surface Analogs in Pd0.18Cu15 Nanoparticles for Selective Hydrogenation Reactions. *Phys. Chem. Chem. Phys.* **2013**, *15*, 12187−12196.
(21) Pei, G. X.; Liu, X. Y.; Wang, A.; Li, L.; Huang, Y.; Zhang, T.; Lee, J. W.; Jang, B. W. L.; Mou, C.-Y. Promotional Effect of Pd Single Atoms on Au Nanoparticles Supported on Silica for the Selective Hydrogenation of Acetylene in Excess Ethylene. *New J. Chem.* **2014**, *38*, 2043−2051.
(22) Pei, G. X.; Liu, X. Y.; Yang, X.; Zhang, L.; Wang, A.; Li, L.; Wang, H.; Wang, X.; Zhang, T. Performance of Cu-Alloyed Pd Single-Atom Catalyst for Semihydrogenation of Acetylene under Simulated Front-End Conditions. *ACS Catal.* **2017**, *7*, 1491−1500.
(23) Xie, W.; Xu, J.; Ding, Y.; Hu, P. Quantitative Studies of the Key Aspects in Selective Acetylene Hydrogenation on Pd(111) by Microkinetic Modeling with Coverage Effects and Molecular Dynamics. *ACS Catal.* **2021**, *11*, 4094−4106.
(24) Liu, J.; Uhlman, M. B.; Montemore, M. M.; Trimpalis, A.; Giannakakis, G.; Shan, J.; Cao, S.; Hannagan, R. T.; Sykes, E. C. H.; Flytzani-Stephanopoulos, M. Integrated Catalysis-Surface Science-Theory Approach to Understand Selectivity in the Hydrogenation of 1-Hexyne to 1-Hexene on PdAu Single-Atom Alloy Catalysts. *ACS Catal.* **2019**, *9*, 8757−8765.
(25) van der Hoeven, J. E. S.; Ngan, H. T.; Taylor, A.; Eagan, N. M.; Aizenberg, J.; Sautet, P.; Madix, R. J.; Friend, C. M. Entropic Control of HD Exchange Rates over Dilute Pd-in-Au Alloy Nanoparticle Catalysts. *ACS Catal.* **2021**, *11*, 6971−6981.
(26) Dumesic, J. A. Analyses of Reaction Schemes Using De Donder Relations. *J. Catal.* **1999**, *185*, 496−505.
(27) Campbell, C. T. The Degree of Rate Control: A Powerful Tool for Catalysis Research. *ACS Catal.* **2017**, *7*, 2770−2779.
(28) Mao, Z.; Campbell, C. T. Apparent Activation Energies in Complex Reaction Mechanisms: A Simple Relationship via Degrees of Rate Control. *ACS Catal.* **2019**, *9*, 9465−9473.
(29) van der Hoeven, J. E. S.; Ngan, H. T.; Yan, G.; Aizenberg, J.; Madix, R. J.; Sautet, P.; Friend, C. M. Unraveling 1-Hexene Hydrogenation over Dilute Pd-in-Au Alloys. *J. Phys. Chem. C* **2022**, *126*. DOI: 10.1021/acs.jpcc.2c04982.
(30) Canduela-Rodriguez, G.; Sabbe, M. K.; Reyniers, M.-F.; Joly, J.-F.; Marin, G. B. Thermodynamic Study of Benzene and Hydrogen Coadsorption on Pd(111). *Phys. Chem. Chem. Phys.* **2014**, *16*, 23754−23768.
(31) Darby, M. T.; Sykes, E. C. H.; Michaelides, A.; Stamatakis, M. Carbon Monoxide Poisoning Resistance and Structural Stability of Single Atom Alloys. *Top. Catal.* **2018**, *61*, 428−438.
(32) Darby, M. T.; Réocreux, R.; Sykes, E. H.; Michaelides, A.; Stamatakis, M. Elucidating the Stability and Reactivity of Surface Intermediates on Single-Atom Alloy Catalysts. *ACS Catal.* **2018**, *8*, 5038−5050.
(33) Li, H.; Chai, W.; Henkelman, G. Selectivity for Ethanol Partial Oxidation: The Unique Chemistry of Single-Atom Alloy Catalysts on Au, Ag, and Cu(111). *J Mater Chem A Mater* **2019**, *7*, 23868−23877.
(34) Hammer, B.; Norskov, J. K. Why Gold Is the Noblest of All the Metals. *Nature* **1995**, *376*, 238−240.
(35) Xin, H.; Vojvodic, A.; Voss, J.; Nørskov, J. K.; Abild-Pedersen, F. Effects of d -Band Shape on the Surface Reactivity of Transition-Metal Alloys. *Phys Rev B Condens Matter Mater Phys* **2014**, *89*, 115114.
(36) Kresse, G.; Hafner, J. Ab Initio Molecular Dynamics for Liquid Metals. *Phys. Rev. B* **1993**, *47*, 558−561.
(37) Kresse, G.; Hafner, J. Ab Initio Molecular-Dynamics Simulation of the Liquid-Metalamorphous- Semiconductor Transition in Germanium. *Phys. Rev. B* **1994**, *49*, 14251−14269.
(38) Dion, M.; Rydberg, H.; Schröder, E.; Langreth, D. C.; Lundqvist, B. I. Van Der Waals Density Functional for General Geometries. *Phys. Rev. Lett.* **2004**, *92*, 246401.
(39) Román-Pérez, G.; Soler, J. M. Efficient Implementation of a van Der Waals Density Functional: Application to Double-Wall Carbon Nanotubes. *Phys. Rev. Lett.* **2009**, *103*, 096102.
(40) Klimeš, J.; Bowler, D. R.; Michaelides, A. Chemical Accuracy for the van Der Waals Density Functional. *J. Phys.: Condens. Matter* **2009**, *22*, 022201.
(41) Gautier, S.; Steinmann, S. N.; Michel, C.; Fleurat-Lessard, P.; Sautet, P. Molecular Adsorption at Pt(111). How Accurate Are DFT Functionals? *Phys. Chem. Chem. Phys.* **2015**, *17*, 28921−28930.
(42) Koeleman, B. J. J.; de Zwart, S. T.; Boers, A. L.; Poelsema, B.; Verhey, L. K. Adsorption Study of Hydrogen on a Stepped Pt (997) Surface Using Low Energy Recoil Scattering. *Nucl. Instrum. Methods Phys. Res.* **1983**, *218*, 225−229.
(43) Norton, P. R.; Davies, J. A.; Jackman, T. E. Absolute Coverage and Isosteric Heat of Adsorption of Deuterium on Pt(111) Studied by Nuclear Microanalysis. *Surface Science Letters* **1982**, *121*, A364.
(44) Monkhorst, H. J.; Pack, J. D. Special Points for Brillouin-Zone Integrations. *Phys Rev B Condens Matter Mater Phys* **1976**, *13*, 5188−5192.
(45) Methfessel, M.; Paxton, A. T. High-Precision Sampling for Brillouin-Zone Integration in Metals. *Phys. Rev. B* **1989**, *40*, 3616−3621.

(46) Henkelman, G.; Jónsson, H. A Dimer Method for Finding Saddle Points on High Dimensional Potential Surfaces Using Only First Derivatives. *J. Chem. Phys.* **1999**, *111*, 7010−7022.
(47) Momma, K.; Izumi, F. VESTA 3 for Three-Dimensional Visualization of Crystal, Volumetric and Morphology Data. *J. Appl. Crystallogr.* **2011**, *44*, 1272−1276.
(48) Marcella, N.; Lim, J. S.; Płonka, A. M.; Yan, G.; Owen, C. J.; van der Hoeven, J. E. S.; Foucher, A. C.; Ngan, H. T.; Torrisi, S. B.; Marinkovic, N. S.; Stach, E. A.; Weaver, J. F.; Aizenberg, J.; Sautet, P.; Kozinsky, B.; Frenkel, A. I. Decoding Reactive Structures in Dilute Alloy Catalysts. *Nat. Commun.* **2022**, *13*, 832.
(49) Gokhale, A. A.; Kandoi, S.; Greeley, J. P.; Mavrikakis, M.; Dumesic, J. A. Molecular-Level Descriptions of Surface Chemistry in Kinetic Models Using Density Functional Theory. *Chem. Eng. Sci.* **2004**, *59*, 4679−4691.
(50) Cortright, R. D.; Dumesic, J. A. Kinetics of Heterogeneous Catalytic Reactions: Analysis of Reaction Schemes. *Adv. Catal.* **2001**, *46*, 161−264.
(51) Wang, T.; Ibañez, J.; Wang, K.; Fang, L.; Sabbe, M.; Michel, C.; Paul, S.; Pera-Titus, M.; Sautet, P. Rational Design of Selective Metal Catalysts for Alcohol Amination with Ammonia. *Nat Catal* **2019**, *2*, 773−779.
(52) Luneau, M.; Guan, E.; Chen, W.; Foucher, A. C.; Marcella, N.; Shirman, T.; Verbart, D. M. A.; Aizenberg, J.; Aizenberg, M.; Stach, E. A.; Madix, R. J.; Frenkel, A. I.; Friend, C. M. Enhancing Catalytic Performance of Dilute Metal Alloy Nanomaterials. *Commun Chem* **2020**, *3*, 46.
(53) Harrison, A. G.; Jones, E. G.; Gupta, S. K.; Nagy, G. P. TOTAL CROSS SECTIONS FOR IONIZATION BY ELECTRON IMPACT. *Can. J. Chem.* **1966**, *44*, 1967−1973.
(54) Brown, S. T.; Buitrago, P.; Hanna, E.; Sanielevici, S.; Scibek, R.; Nystrom, N. A. Bridges-2: A Platform for Rapidly-Evolving and Data Intensive Research. *Practice and Experience in Advanced Research Computing*; ACM: New York, NY, USA, 2021, pp 1−4.
(55) Towns, J.; Cockerill, T.; Dahan, M.; Foster, I.; Gaither, K.; Grimshaw, A.; Hazlewood, V.; Lathrop, S.; Lifka, D.; Peterson, G. D.; Roskies, R.; Scott, J. R.; Wilkins-Diehr, N. XSEDE: Accelerating Scientific Discovery. *Comput Sci Eng* **2014**, *16*, 62−74.

https://doi.org/10.1021/acscatal.2c03560
ACS Catal. 2022, 12, 13321−13333